Fused and Cascaded Squeeze Excitation Network for Pneumonia Detection

Ramitha M. A.[1], N. Mohanasundaram[2], R. Santhosh[3,*]

[1]Research Scholar, Department of Computer Science and Engineering, Karpagam Academy of Higher Education, Coimbatore, Tamil Nadu, India

[23]Professor, Department of Computer Science and Engineering, Karpagam Academy of Higher Education, Coimbatore, Tamil Nadu, India

[3] Professor, Department of Computer Science and Engineering, Faculty 0f Engineering, Karpagam Academy of Higher Education, Coimbatore, Tamil Nadu, India

Emails: karpagam.publication@gmail.com; itismemohan@gmail.com; santhoshrd@gmail.com

Abstract

Pneumonia is a medical condition affecting 100 million people globally, and rates are predicted to reach epidemic levels within the next several decades. As a result of the air sacs in both or even one lung becoming inflamed, the patient may experience fever, chills, and trouble breathing. Coughs with pus may also occur. Various organisms can cause pneumonia, including bacteria, viruses, and fungi. Early detection of pneumonia can allow the severity of the purulent material to be reduced. The ability of computer-aided detection techniques to reliably diagnose pneumonia has made them popular among scientists. We used a pre-trained Inception V3Net, Squeeze Excitation-based deep Convolutional Neural Network (SE-CNN) that was trained on the Kermany dataset and the RSNA Pneumonia Detection Challenge dataset in this study. In early-stage detection, the suggested technique beat previous state-of-the-art networks, achieving 91% precision in severity rating. Furthermore, our network's accuracy, recall, f1-score, as well as quadratic weighted kappa were reported to be 91.56%, 91%, and 90%, respectively. In terms of processing time and space, our suggested framework is simple, precise, and effective.

Keywords: Deep learning, CNN; Fused & Excitation block; Pneumonia; Squeeze Excitation based deep Convolutional Neural Network

1. Introduction

Throughout history, numerous outbreaks and chronic illnesses have resulted in significant loss of life and caused major crises that required significant time and effort to overcome. When discussing diseases that occur within a population during a specific timeframe, the terms "epidemic" and "outbreak" are commonly used. Worldwide, more than 1 million people contract pneumonia each year, unfortunately resulting in 50,000 deaths annually. Factors such as age, smoking, alcohol consumption, and malnutrition can all contribute to an individual's risk of developing pneumonia. While pneumonia can affect people of all ages, it poses a greater risk to those with weakened immune systems, particularly infants under the age of two and adults aged 65 and older [1]. Fortunately, with prompt diagnosis and treatment, pneumonia can be effectively managed as a disease. Pneumonia is a potentially fatal microbial infection that damages the lungs, and it is caused by the bacteria called “Streptococcus pneumonia”. As per the World Health Organization

Doi: https://doi.org/10.54216/FPA.160110

Received: July 15, 2023 Revised: November 15, 2023 Accepted: April 28, 2024

(WHO), pneumonia accounts for one-third of all deaths in India. Expert radiotherapists examine chest X-rays to determine pneumonia.

The best approach for detecting pneumonia is presently chest X-rays [1]. But the diagnosing pneumonia from chest X-ray images is hard even by a specialist. A pneumonia X-ray is blurry and is often misinterpreted as an illness or benign anomaly. Pneumonia detection through X-ray images is often uncertain due to the possibility of confusion with other diseases and benign abnormalities. As a result, this lack of clarity has led to significant subjectivity in the diagnostic decisions made by radiologists, resulting in variations in the diagnosis of pneumonia. Because of specialist misclassifications, some patients are given incorrect drugs [2-4]. In low-resource countries, there are also fewer qualified radiologists, particularly in rural areas, which can lead to subjective judgments in the radiology diagnosis of pneumonia. As a result, there is a high need for Computer-Aided Diagnosis systems that may help radiologists easily distinguish between various pneumonia types from chest X-ray images (Figure 1) + (CAD) has emerged as a prominent study subject in machine learning in recent years. The CAD system is mainly developed to reduce the double reading cost and detection error and to enhance radiologists' performance. Thus, it saves the patient's life. The complexity of pneumonia and the large amount of available data from examinations of pneumonia infections leads to develop CAD. Existing CAD systems have previously been shown to aid in the identification of breast cancer, mammography, lung nodules, and other medical conditions. Because of the efficiency of deep learning techniques in analyzing clinical images, Computer-Aided Designs are used mostly for categorizing illness [5].

pre-trained Computer-Aided Design models on large datasets help to immensely improve image classification tasks. The use of deep learning (DL) and machine learning (ML) to identify chest X-rays is gaining traction because a variety of ML models can be trained on a huge amount of data, and they are simple to implement. Artificial intelligence is a vital tool that plays a critical role in resolving many intricate computers vision challenges. One specific type of artificial intelligence, DL models, particularly convolutional neural networks (CNNs), are utilized for different image classification tasks. The performance of these models is optimal only when presented with a vast amount of data. Obtaining a large quantity of labeled data for biomedical image classification is challenging and costly because it necessitates the involvement of skilled medical professionals to manually classify each image, which is a time-intensive task. To overcome this obstacle, transfer learning is used. A common approach in deep learning is to transfer the knowledge learned from a pre-trained model on a large dataset to solve a problem with a smaller dataset. This involves applying the network weights obtained from the pre-trained model. For biomedical image classification, CNN models trained on massive datasets such as ImageNet, which contains more than 14 million images, are often utilized. Numerous studies have investigated deep machine learning algorithms for identifying pneumonia.

Most of the studies have reported high classification performance, as indicated by accuracy, recall, precision, and F1-measure. However, it should be noted that most of these classification models were trained and tested on relatively small datasets. Due to this dataset size limitation, the proposed models serve more as a proof-of-concept for pneumonia detection, and therefore necessitate re-evaluation with larger datasets to validate their efficacy. Thus, a novel automatic CAD is created and developed in this work to aid the radiologist in accurately recognizing potential suspicious lesions. In this research, we consider building DL based classification models to detect pneumonia. Some of the existing models of CAD for the breast image classification process are described in section 2

1.1 Key Highlights

This paper finds an effective DL model for classifying pneumonia in which following are the objectives.

- Develop a deep-learning model for the effective detection and classification of pneumonia
- With the help of chest X-ray images, DL model has been performed
- Usage of fused and excitation block of squeeze network effectively detects the pneumonia
- Experiment evaluation has been conducted in which the proposed system outperforms over various measures.

Doi: https://doi.org/10.54216/FPA.160110

Received: July 15, 2023 Revised: November 15, 2023 Accepted: April 28, 2024

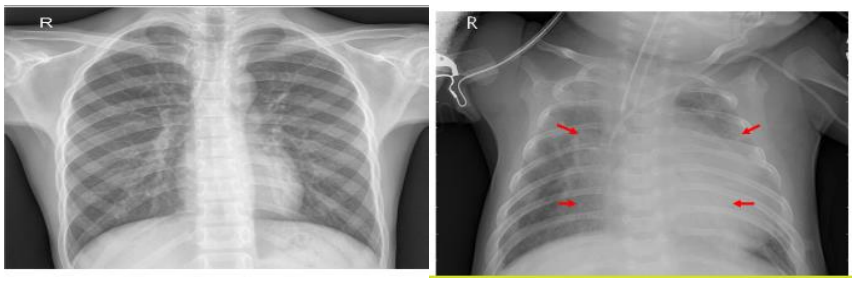

Figure 1: Examples of two x-ray images (a) healthy lung and (b) pneumonic lung

Organization of paper: Section 1 gives the overview of pneumonia and related information, Section 2 depicts the literature review, Section 3 depicts the overall methodology, Section 4 depicts the performance analysis and finally ends with conclusion in Section 5.

2. Related Works

Exploration of Machine Learning methods in identifying thoracic disorders has gotten a lot of interest recently in the field of medical picture categorization research. Lakhani et al (2017) [6] suggested a technique for identifying TB in the lungs based on the architectures of two separate DCNNs, AlexNet and GoogleNet. Huang et al. devised a lung nodule categorization system for diagnosing lung cancer. [7] used deep learning techniques as well. In their study [8], Islam et al. evaluated various types of CNN for finding anomalies in chest X-rays using OpenI dataset [9.]. Varshini et al suggested a strategy to classify abnormal and normal chest X-rays based on CNN models, as proposed by Wang et al. (2017) [10]. According to his findings, pre-trained CNN models and supervised classifier algorithms are highly useful for diagnosing lung diseases, particularly pneumonia, based on X-ray images. Rashman et al. [11] developed a technique for diagnosing bacterial and viral pneumonia with the use of digital x-rays. The authors first provide a comprehensive analysis of developments in pneumonia diagnosis and then describe the authors' method. For transfer learning, AlexNet, Residual networks, etc were utilized. For this study, Kumar et al. obtained X-ray images of pneumonia patients with afflicted and unaffected chests and used Convolutional Neural Networks (CNNs) in various configurations to perform an ML-based binary classification task. Based on the fine correlation between minimal level loss and accuracy, the paper compares results from different simple CNN frameworks and selects the most accurate design. A chest X-ray cannot be used to treat bacterial, fungal, viral, or community-acquired pneumonia, but it can serve as a valuable diagnostic tool for detecting bacterial, fungal, viral, and community-acquired pneumonia. Table 1 depicts the overall summary of authors on pneumonia detection.

Table 1: Related Works over pneumonia detection

S.No	Ref.	Techniques	Benefits	Limitations
1	[13]	Pre-trained CNN for classification based on ImageNet.	Fast-learning techniques can be applied even to deep CNNs.	A negative transfer from ImageNet can occur if the CXRs are not the same as CNN since CNN has been pretrained on a different dataset.
2	[14]	Disease identification with 121-layer CNNs based on localization	The localization of pathology by density produces a reasonable amount of information outcome.	Use only frontal radiographs for diagnosis, since lateral views are not usually needed for diagnosis.
3	[15]	Genetic classifiers distinguish between UIP and non-UIP using logistic regression.	Specificity of 0.86 and AUC of 0.86 are excellent values.	The test considers less people for testing. the sensitivity is 0.63 which is low.

Doi: https://doi.org/10.54216/FPA.160110

Received: July 15, 2023 Revised: November 15, 2023 Accepted: April 28, 2024

4	[16]	An additive model that is easily understandable was used for pneumonia identification.	The technique they have developed can result in comprehensible and accurate output.	the precise rationale for the predictions remains unclear (different factors: overfitting, variable correlation, etc.).
5	[17]	Pretrained CNNs used for heatmap localization based on a CXR-based dataset for thoracic diseases	We created and analyzed a large and diversified dataset of frontal CXRs of 32,718 patients (108,948 unique CXRs).	Using data mining, ground-truth labels were attained, which were determined by the judgment of a single radiologist. There may be ambiguities in how diseases are seen on CXRs, which could lead to errors in the ground truth.
6	[18]	An ensemble pathology detection model was constructed using Mask RCNN and RetinaNet.	When it comes to disease localization, deep ensemble learning provides an excellent MAP.	Each model requires a lot of CPU time to train and is a challenge. Work exclusively uses frontal CXRs and does not utilize lateral CXRs, which is a drawback.
7	[18]	It applied a four-layer-CNN for the identification of pneumonia.	An accuracy of 93% is achieved using a simple CNN architecture.	Despite the importance of experimental analysis accuracy, Precision and recall are not included in the study.

Sain et al. [19] created a CNN model for classification and diagnosing pneumonia in chest X-ray Images. For diagnosis, they use several data augmentation approaches, changes in the learning rate, and annealing to minimize overfitting and reduce generalization error due to the short dataset size. The author was inspired to design a strategy for properly recognizing the presence/absence of pneumonia from chest images after reviewing the above-mentioned pieces of literature on the subject.Research has previously emphasized that CNNs can be used as deep learning frameworks to diagnose pneumonia, according to the literature. In the case of negative transfers with a high level of uncertainty, however, optimizing transfer learning methods can be difficult since the models are typically pre-trained in a classifier with large numbers of images, such as the ImageNet. Models are trained on many pictures. Using transfer learning for designs that need more training time can likely help the model converge faster. To address these issues, the study proposed a Squeeze Excitation network-based deep Convolution Neural Network (SE-CNN) architecture for extracting characteristics from chest X-ray pictures and classifying them to determine if a person has pneumonia. To see how the amount of the dataset affects SE-CNN performance, the suggested SE-CNNs are trained using both the original and supplemented datasets, and the results are shown. The findings show that, when compared to their larger architectural counterparts, smaller SE-CNN designs may attain state-of-the-art accuracy while also having shorter training periods and reduced computing costs.

3. Proposed Work

First, we'll go through the recommended architectures for classifying chest X-ray images to diagnose pneumonia in this part. It is an issue of binary classification. The SENet blocks are connected back-to-back, and the last two blocks are used as side outputs. The second SENet's side output (feature map of the second SENet) is downsampled (average pooling). The side output from the third SENet block is concatenated with the downsampled features. The softmax classifier is fed these results as shown in architecture Figure 2.

Doi: https://doi.org/10.54216/FPA.160110

Received: July 15, 2023 Revised: November 15, 2023 Accepted: April 28, 2024

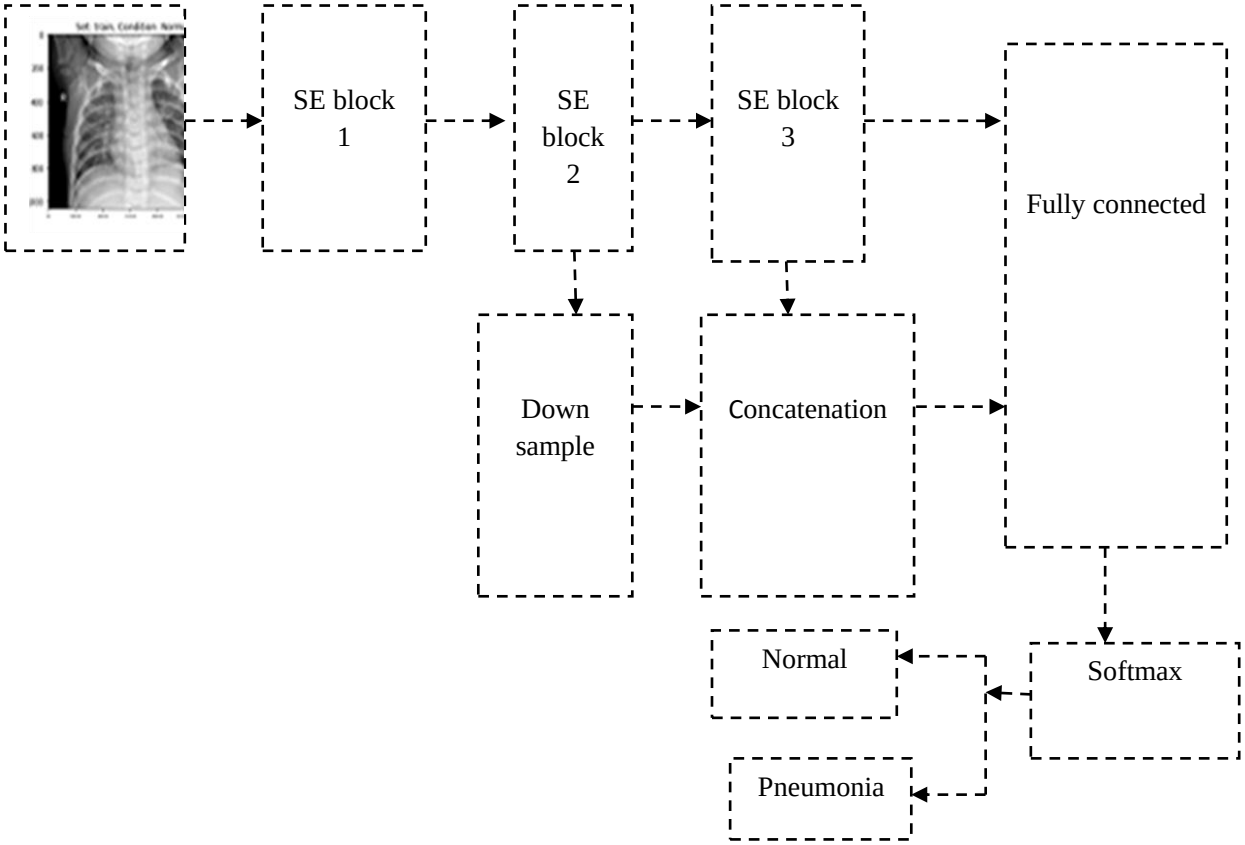

Figure 2: representation of proposed pneumonia detection framework

3.1 Squeeze- Excitation block

After initial aggregated features maps are created for each transformation (F_{tr}), channel descriptors are derived from the input X, converting it to features maps U where $U \epsilon 2\ R^{H\times W\times C}$. Using this descriptor, each level of the network can use the global receptive field to incorporate a global distribution of feature replies. To accomplish this, a simple self-gating mechanism (after aggregation) is used. A set of modulation weights is generated for each channel from the embedded image. Feature maps U are weighted and input into SE blocks (Figure 3) so that the output can be immediately fed into the following layers [21].

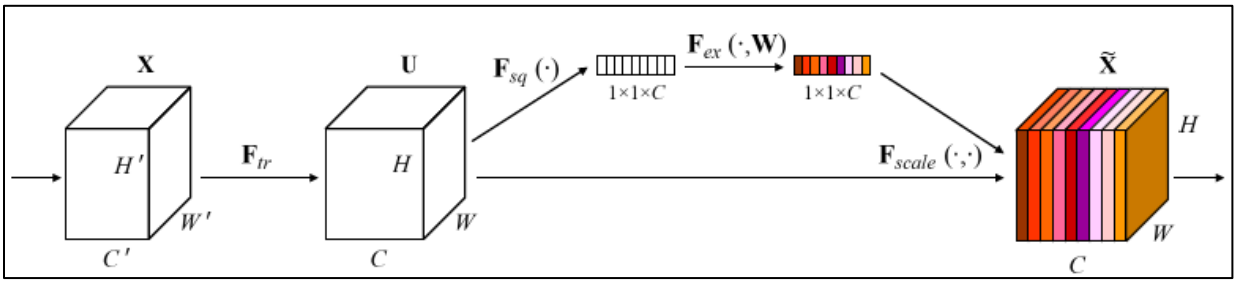

Figure 3: Architecture of Squeeze-and-Excitation Block

Doi: https://doi.org/10.54216/FPA.160110

Received: July 15, 2023 Revised: November 15, 2023 Accepted: April 28, 2024

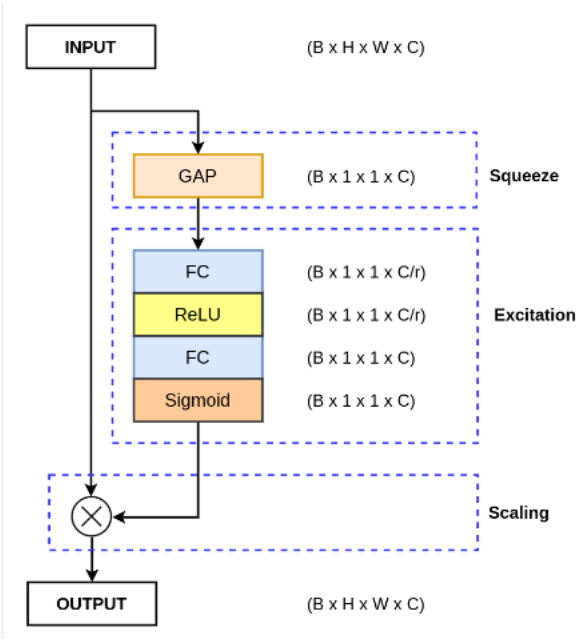

Figure 3(a): Blocks of Squeeze-and-Excitation

The Squeezenext baseline architecture is constructed using bottleneck modules implemented in four stages, which includes a squeeze stage, an excitation scaling stage, and an output stage, as well as a four-stage block configuration. This architecture achieves a favorable balance between accuracy and size when compared to the Squeezenet baseline architecture. Figure 3 (a) depicts the configuration of the Squeezenext baseline architecture.

Squeeze-and-Excitation blocks are computational units based on mappings of inputs $X \epsilon 2\ R^{(H' \times W' \times C')}$ to feature mappings $U\ \epsilon 2\ R^{H \times W \times C}$. F_{tr} denotes convolutional operator V = $[v_1, v_2 \ldots . v_c]$ represents filter Kernels. outputs $U = [u_1;\ u_2; \ldots . u_C]$,

$$u_C = v_c * X = \sum_{s=1}^{C'} v_c^s * X^s \qquad (1)$$

Here $*$ denotes convolution, $v_c = [v_c^1\ ;\ v_c^2; :::;\ v_c^s\ ]$, $X = [x^1;\ x^2; :::;\ x^{c'}\ ]$ and $U\ \epsilon 2\ R^{H \times W \times C}$. v_c is 2D spatial kernel that denotes a single v_c channel acting on the matching X-channel. Because the output is computed by adding the results of all channels together, we can take advantage of bias-free notation here. Channel interdependencies are effectively incorporated into v_c, although they also interact with the localized correlation calculated through the filters. Since the output is derived from summating over all channels, there is implicit incorporation of channel dependence into v_c, though the local spatial correlation is also gathered through the filters, so they are also closely interconnected. Explicit modeling of channel interactions strengthens the ability of the network to learn convolutional features, enabling later transformations to take advantage of information that was unexplored before [22]. so tune filter responses can be provided in two stages, squeezing and excitement, before getting into the next transformation. Figure 2 shows the construction of a SE block.

3.2 Squeeze: Global Information Embedding

Looking at the output features first, we can determine whether channel dependencies exist. Due to the limited receptive fields of the learned filters, each output unit of the transformation cannot use any context outside it. By generating channel-specific data via global average pooling, we can compress the spatial information of the globe into the description of a particular channel. A statistic $z\epsilon\ 2\ R^C$ is created by decreasing U through its spatial dimension $T\ \times K$, such that, 'z' is computed by c-th element

Doi: https://doi.org/10.54216/FPA.160110

Received: July 15, 2023 Revised: November 15, 2023 Accepted: April 28, 2024

$$z_c = F_{sq}(u_c) = \frac{1}{H \times W}\sum_{i=1}^{H}\sum_{j=1}^{W} u_c(i,j) \qquad (2)$$

3.3 Excitation: Adaptive Recalibration

With the information obtained we follow up the squeeze operation with a second operation that aims to fully capture channel-wise dependencies (Figure 4). The function needs to meet two requirements to fulfill this objective: first, it must be flexible and secondly, because multiple channels should be put together, it must learn a no mutually exclusive relationship. A gating system is used with sigmoid activation to obtain these requirements:

$$s = F_{ex}(z, W) = \sigma\big(g(z, W)\big) = \sigma(W_2\delta(W_1 z)) \qquad (3)$$

here δ denotes the ReLU [23] function,$W_1 \in R^{\frac{C}{r}\times C}$ C and $W_2 \in R^{C\times\frac{C}{r}}$. Two Fully Connected layers (FC) form the bottleneck for parameterizing the gating mechanism. The model will be simplified and generalized by reducing the dimensionality to r and increasing the channel dimension of the transformation output U via a dimensionality reduction layer. It is possible to derive the block's ultimate output by rescaling U with activations s:

$$x_c^{\check{}} = F_{scle}(u_c, s_c) = s_c u_c \qquad (4)$$

where $X = [X_1^{\check{}}, X_2^{\check{}}, \ldots X_c]$ and $F_{scle}(u_c, s_c)$ gives the channel-wise multiplication value between the feature map $U_c \in 2\ R^{H\times W}$ and the scalar s_c

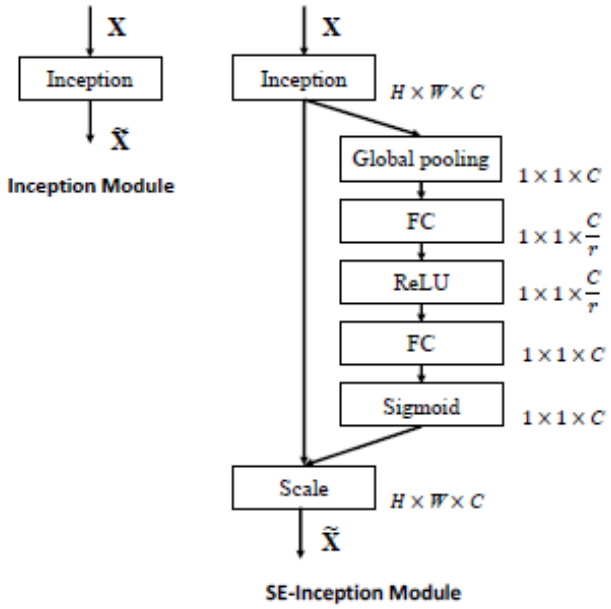

Figure 4: This diagram illustrates the schemas of the Left: SEInception module, Right: original Inception module.

Doi: https://doi.org/10.54216/FPA.160110

Received: July 15, 2023 Revised: November 15, 2023 Accepted: April 28, 2024

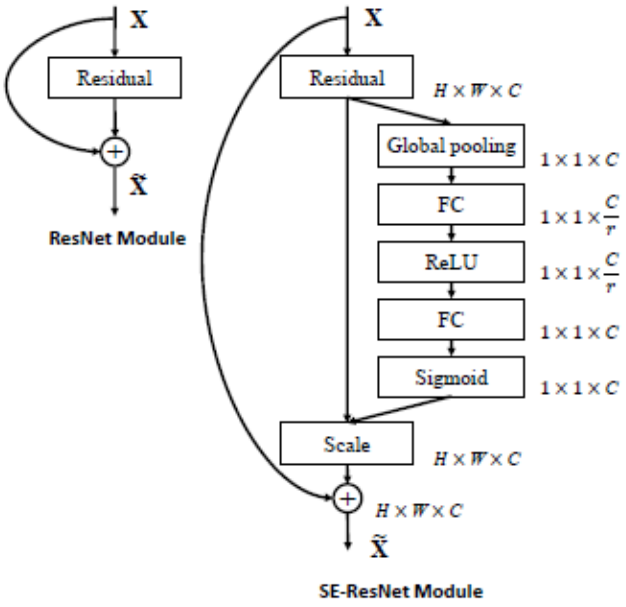

Figure 5: The Residual module and the SEResNet module (left and right).

A traditional design, such as VGGNet [24], would insert the SE block after each non-linear convolution. The SE block is quite adaptable, allowing it to be used for transformations than standard convolutions directly. The SE blocks of Inception networks is builds first [25]. For instance, changing F_{tr} to a complete Inception module as shown in Fig. 3 and repeating this process for every module would result in a SE Inception network. The non-identity branch of a residual module represents the SE block transformation F_{tr}in Figure 5. Additional SE blocks can be used to build residual nets (Fig. 4). Convolutional nuclei, where each neuron serves as a nucleus, act before aggregation with the identity branch. When a kernel is symmetric, a convolution operates as a correlation. An image is sliced into tiny pieces called receptive fields by the convolutional kernel:

$$f_1^k(p,q) = \sum_c \sum_{x,y} i_c(x,y) \,.\, e_1^k(u,v) \qquad (5)$$

An example of a convolutional outcome feature vector is$F_1^k = [f_1^k(1,1), \dots (f_1^k(p,q), .. f_1^k(P,Q))]$.

As long as their relative positions to each other are preserved, property placement in the pooling layer becomes less important. Downsampling is a fun local activity. It takes identical data from the surrounding region of the receiving field and generates the dominant response in that area.

$$Z_l^k = g_p\left(F_l^k\right) \qquad (6)$$

Equation (2) depicts the pooling operation, with Z_l^k representing the feature-map of the pooling of l[th] layer for the k[th] input feature-map $F_l^k$and $g_p(.)$ denoting the pooling operation type. The pooling technique allows for the extraction of a mixture of characteristics that are insensitive to slight distortions and translational shifts. Equation (7) defines the activation function of a convoluted feature map.

$$T_l^k = g_a(F_l^k) \qquad (7)$$

Convolution is used to get the F_l^k output, it is subsequently allocated to the function of the activation $g_a(.)$, This introduces non-linearity and results in the transition $T_l^k$for the lth layer.

Doi: https://doi.org/10.54216/FPA.160110

Received: July 15, 2023 Revised: November 15, 2023 Accepted: April 28, 2024

In Softmax, a vector of values is converted into a vector of probability, with the probability that each pixel will have that value significantly correlated to the vector's relative scale. This concept is then expanded into a multiclass universe. When there are multiple classes, Softmax assigns each one a decimal probability. The decimal probabilities sum must equal 1.0. This additional restriction makes training converge more quickly than otherwise. In the Softmax layer, the ANN is used before the output layer. There must be the same no of nodes in the Softmax layer as in the output layer.

$$softmax(z_i) = \frac{\exp(z_i)}{\sum_j \exp(z_j)} \qquad (8)$$

3.4 Validation and Confusion Metrics

The performance analysis of the classification model is clearly defined using a 'confusion matrix.' The factors in that matrix can be summarized as follows,

- TP (True Positives): Number of chest images of pneumonia/ normal that are marked as images of non-pneumonia/ normal.
- TN (True Negatives): Images of pneumonia/ normal chest are known as images of non-pneumonia/ normal.
- FP (False Positives): Number of images categorized as pneumonia/ normal that are non-pneumonia/ normal.
- False Negatives (FN): Number oof pneumonia/ normal chest marked as pneumonia/ normal.

$$Precision = \frac{TP1}{TP1+FP1} \times 100\% \qquad (9)$$

$$F-measure = \frac{2*Precision*Recall}{Precision+Recall} \qquad (10)$$

$$Recall = \frac{TP1}{TP1+FN1} \qquad (11)$$

$$Accuracy = \frac{TP1+TN1}{TP1+FP1+FN1+TN1} \times 100\% \qquad (12)$$

From True Labels and Expected Labels, the Confusion Graph creates a Graph of the Confusion Matrix. Expected Labels returns the Confusion Matrix as a Graph. According to the confusion matrix, the rows are the actual classification, while the columns are the anticipated classification. Off-diagonal cells result in incorrectly classified cases, while diagonal cells result in incorrectly classified cases. Each cell in the confusion matrix of the softmax classifier shows the number of observations for every feature attribute. Confusion matrix rows intimates the actual class, and columns represents the anticipated class. Rightly identified examples are represented by diagonal cells, while incorrectly identified examples are represented by off-diagonal cells. As can be seen from the diagonal part of the confusion matrix, pneumonia/normal pictures are clearly defined. Figure 6 depict the confusion matrix of the proposed model in which out of 5856 images from that dataset, TP = 183, FP= 52, FN = 7and TN = 383.

The training and testing methods are based on the SE-CNN classification, which was determined from the Kermany and RSNA datasets. For validation 60%-40%, 70%-30%, 80%-20%, and 90%-10%of the data is used for training and for testing respectively. The Confusion Matrix is displayed in 6 (a)-6 respectively and their matrices tables are shown in 2 (a)-2 (d).

Doi: https://doi.org/10.54216/FPA.160110

Received: July 15, 2023 Revised: November 15, 2023 Accepted: April 28, 2024

280 46.67%	**20** **3.33%**	**93.3%** **6.7%**
30 **3.57%**	**390** **46.43%**	**92.85%** **7.15%**
90.32% **9.68%**	**91.2%** **8.8%**	**90.16%**

Figure 6 (a) : Classification table 60 : 40 (1080 : 720) (normal : Pneumonia 300 : 420)

Table 6 (a): Metrics

Metrics	Values
Sensitivity	93.33%
Specificity	92.85%
Precision	90.32%
Recall	91.2%
Accuracy	90.16%

270 45%	**30** **5%**	**90%** **10%**
25 **5.21%**	**215** **44.79%**	**89.58%** **10.42%**
91.52% **8.42%**	**87.75%** **12.25%**	**89.91%**

Figure 6 (b): Classification table 70: 30 (1260 : 540) (normal : Pneumonia 300 : 240)

Table 6 (b): Matrics

Metrics	Values
Sensitivity	90%

Doi: https://doi.org/10.54216/FPA.160110

Received: July 15, 2023 Revised: November 15, 2023 Accepted: April 28, 2024

Specificity	89.58%
Precision	91.52%
Recall	87.75%
Accuracy	89.91%

160 44.44%	**20** **5.56%**	**88.89%** **11.11%**
25 **6.95%**	**155** **43.05%**	**86.22%** **13.78%**
86.48% **13.52%**	**88.68%** **11.32%**	**84.82%**

Figure 6 (c): Classification table 80 : 20 (1440 : 360) (normal : Pneumonia 180 : 180)

Table 6 (c): Matrics

Metrics	Values
Sensitivity	88.89%
Specificity	86.22%
Precision	86.48%
Recall	88.68%
Accuracy	84.82%

90 47.36%	**5** **2.64%**	**94.84%** **5.16%**
5 **2.94%**	**80** **47.06%**	**94.12%** **5.88%**

Doi: https://doi.org/10.54216/FPA.160110

Received: July 15, 2023 Revised: November 15, 2023 Accepted: April 28, 2024

94.73% **5.27%**	**91%** **9%**	**91.56%**

Figure 6 (d): Classification table 90:10 (1628:180) (normal : Pneumonia 95: 85)

Table 6 (d): Matrics

Metrics	Values
Sensitivity	94.84%
Specificity	94.12%
Precision	94.73%
Recall	91%
Accuracy	**91.56%**

4. Comparative analysis

A comparison of the proposed models is presented in this section. The computations were performed on a Kaggle kernel with four CPUs and 17 GB of RAM and two CPUs and 14 GB of RAM. The evaluations are presented following the comparison of the suggested models. Two publicly available X-ray pneumonia data sets were analyzed. The Kermany dataset contains 5856 chest X-ray scans representing a wide age range for both adults and children, with the respiratory conditions "Pneumonia" and "Normal" equally distributed. As part of the Kaggle challenge, the RSNA donated the second dataset. This paper evaluated the accuracy, sensitivity, specificity, precision, recall, f1-score, quadratic weighted kappa indices, detection rate, TPR, FPR and confusion matrix applied to the SE methodology used in this case by calculating accuracy, precision, recall, f1-score, quadratic weighted kappa indices, and confusion matrix. The model's performance was also tracked by plotting loss and accuracy curves across the number of epochs.

Table 2: performance values of the proposed classifier

Classes	**60 : 40**	**70 : 30**	**80 : 20**	**90:10**
Sensitivity	93.33	90	88.89	94.84
Specificity	92.85	89.58	86.22	94.12
Precision	90.32	91.52	86.48	94.73
Recall	91.2	87.75	88.68	91
F1-score	89	90	92	91
Accuracy	90.16	89.91	84.82	**91.56**
Macro average	87	88	92	89
Weighted average	90	91	91	90

The model was evaluated using the validation set, which comprises 60%-40%, 70%-30%, 80%-20%, and 90%-10% chest photography photos. We calculated the macro average, the weighted average of accuracy, recall, and f1-score to measure performance using study's classification approach. For two classes, we calculated the macro average, the weighted average of accuracy, f1-score, and recall. According to Table 2, Macro Average and Weighted Average are the suggested system assessments for accuracy, recall, and F1-score. Figure 7 depict the evaluation performance plot across various classes.

Doi: https://doi.org/10.54216/FPA.160110

Received: July 15, 2023 Revised: November 15, 2023 Accepted: April 28, 2024

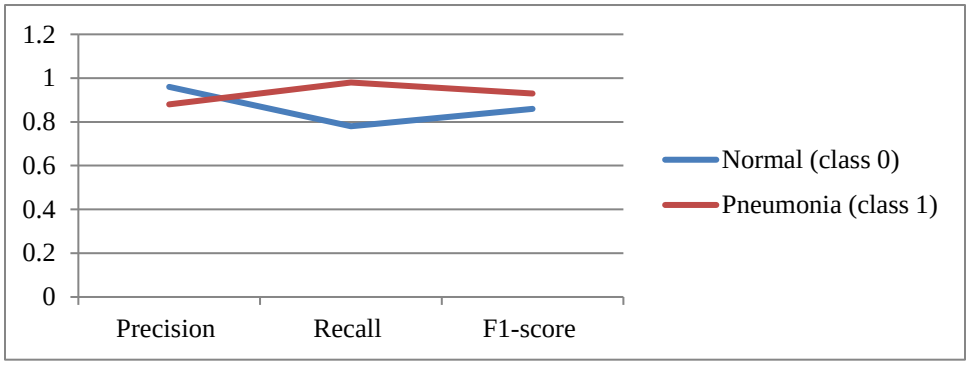

Figure 7: Performance evaluation plot of two classes

According to the best state-of-the-art performance metric for multiclass pneumonia, we use quadratic weighted kappa as our metric for severity rating prediction. In this paper, the Quadratic Weighted Kappa indices for a multi-label classification system are examined and found to be 91.56 %. This method allows for varied weightings of disputes, making it very useful for determining order codes. Figure 8. depicts the Quadratic Weighted Kappa curve as a function of the number of epochs. The suggested method's training and validation accuracy were both determined to be 91.56 %. Figure 9 depict the accuracy and error plot of the proposed model.

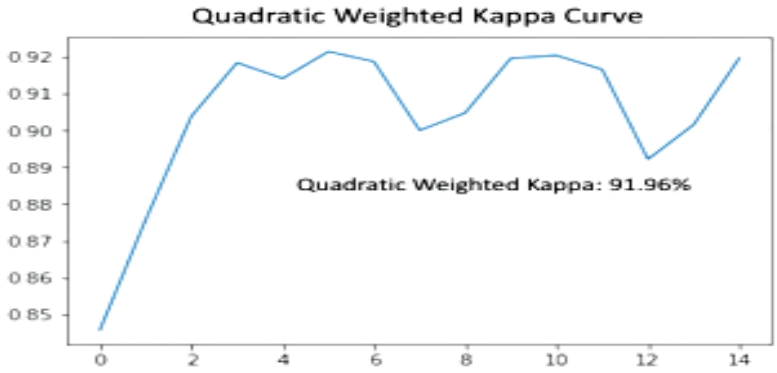

Figure 8: The Quadratic Weighted Kappa curve

Doi: https://doi.org/10.54216/FPA.160110

Received: July 15, 2023 Revised: November 15, 2023 Accepted: April 28, 2024

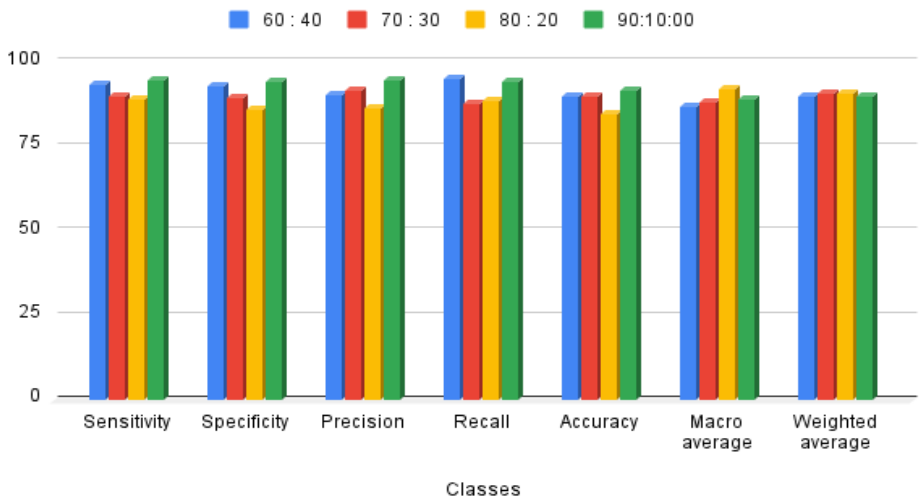

Figure 9: Accuracy and Error plot

Comparison of state art methods

In Table 3, we compare the accuracy and recall of the current study with that of previous studies that have examined classes four and five, and the results range from 37 to 89 % and 30 to 90%, respectively. According to our SE-CNN pneumonia classification, our approach was more accurate and recall was higher than prior computer-aided diagnostic systems. In the identification of pneumonia, we were able to reach a 91.56 % accuracy rate. With respect to recall and specificity proposed model gains better performance (98% and 97%). Figure 9(a,b,c) shows various models over accuracy, sensitivity and recall.

Table 3: Comparison analysis of various models

Reference	Classifier	Accuracy	Recall	Sensitivity
[26]	NN	84	90	93
[27]	SVM	82	82.50	91
[28]	CNN	75	30	94
[29]	CNN	89	76.6	93
[30]	Googlenet	45	-	88
[31]	Googlenet & Alexnet	57.2	-	87
[32]	AlexNet, VGG19, InceptionNet V3	37.43, 50.03, 63.2	-	92
[33]	Ensemble CNN	83.9	-	94
Proposed system	InceptionV3 Net – SE	91.56	96	97

Doi: https://doi.org/10.54216/FPA.160110

Received: July 15, 2023 Revised: November 15, 2023 Accepted: April 28, 2024

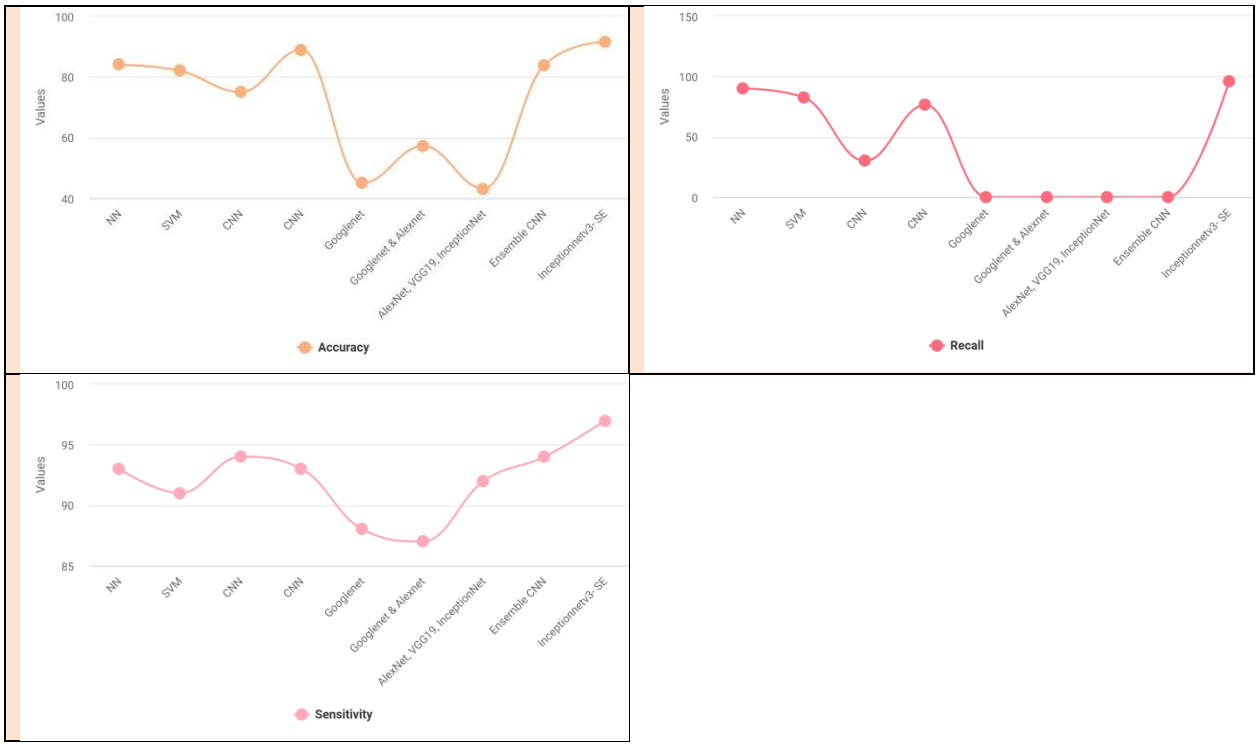

Figure 9: Models vs Measures over a) accuracy, b) Recall, c) sensitivity

Table 4 depict the overall analysis of different models over specificity, precision, and F1-score. Figure 10(a,b,c) shows different models over measures in which proposed model outperforms (specificity: 96, precision:88, F1-score:95).

Table 4: Overall analysis of different models over proposed method

Reference	**Classifier**	**Precision**	**Specificity**	**F1-score**
[26]	NN	82	92	82
[27]	SVM	80	87	78
[28]	CNN	73	81	86
[29]	CNN	87	82	79
[30]	Googlenet	40	93	83
[31]	Googlenet & Alexnet	55	85	84
[32]	AlexNet, VGG19, InceptionNet V3	33.43, 47.03, 60.2	79	87
[33]	Ensemble CNN	80	77	91
Proposed system	InceptionV3 Net – SE	88	96	95

Doi: https://doi.org/10.54216/FPA.160110

Received: July 15, 2023 Revised: November 15, 2023 Accepted: April 28, 2024

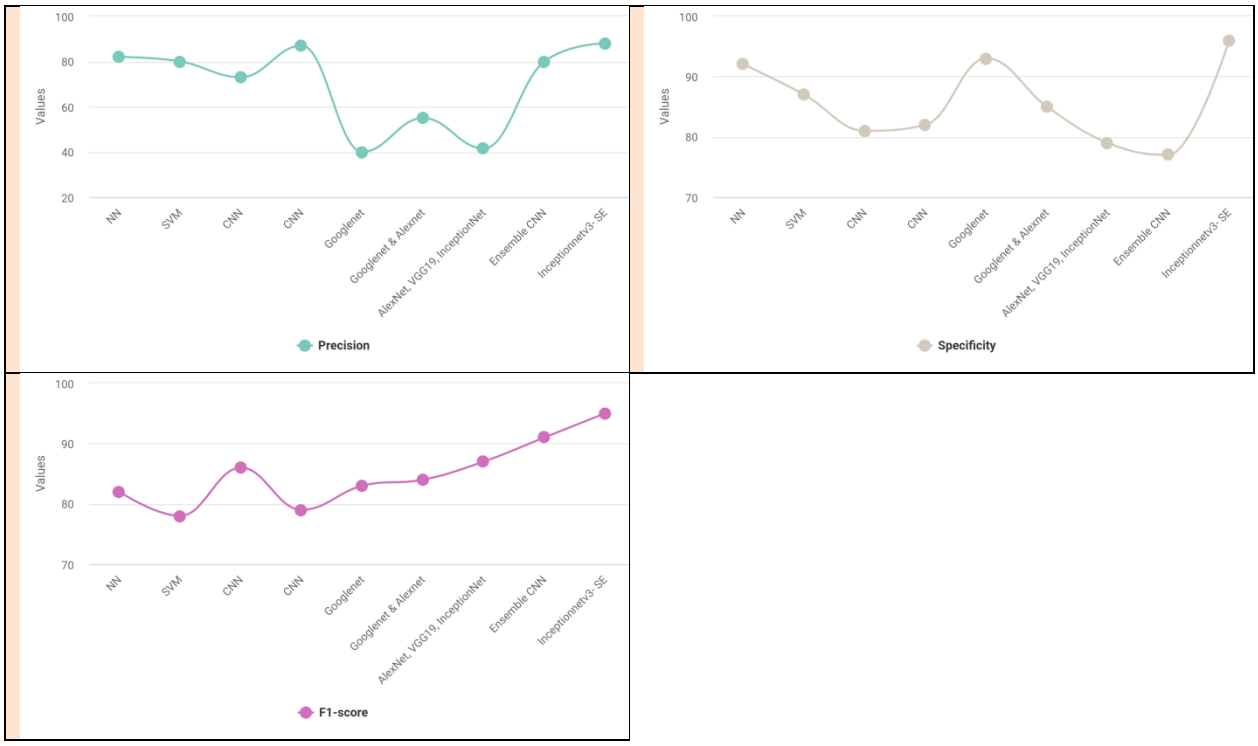

Figure 10.:Models vs Measures over a) Precision, b) Specificity, c) F1-score

Table 5 depict the total analysis of different models over detection rate, TPR and FPR. Figure 11(a,b,c) shows different models over measures in which proposed model performs better than other models (detection rate: 93, TPR: 88, FPR:12).

Table 5: Overall analysis of different models over proposed method

Reference	**Classifier**	**Detection rate**	**TPR**	**FPR**
[26]	NN	81	76	24
[27]	SVM	79	73	27
[28]	CNN	72	69	31
[29]	CNN	86	81	19
[30]	Googlenet	39	28	72
[31]	Googlenet & Alexnet	54	48	52
[32]	AlexNet, VGG19, InceptionNet V3	37.43, 58.03, 57.2	48	52
[33]	Ensemble CNN	84	79	21
Proposed system	InceptionV3 Net – SE	93	88	12

Doi: https://doi.org/10.54216/FPA.160110

Received: July 15, 2023 Revised: November 15, 2023 Accepted: April 28, 2024

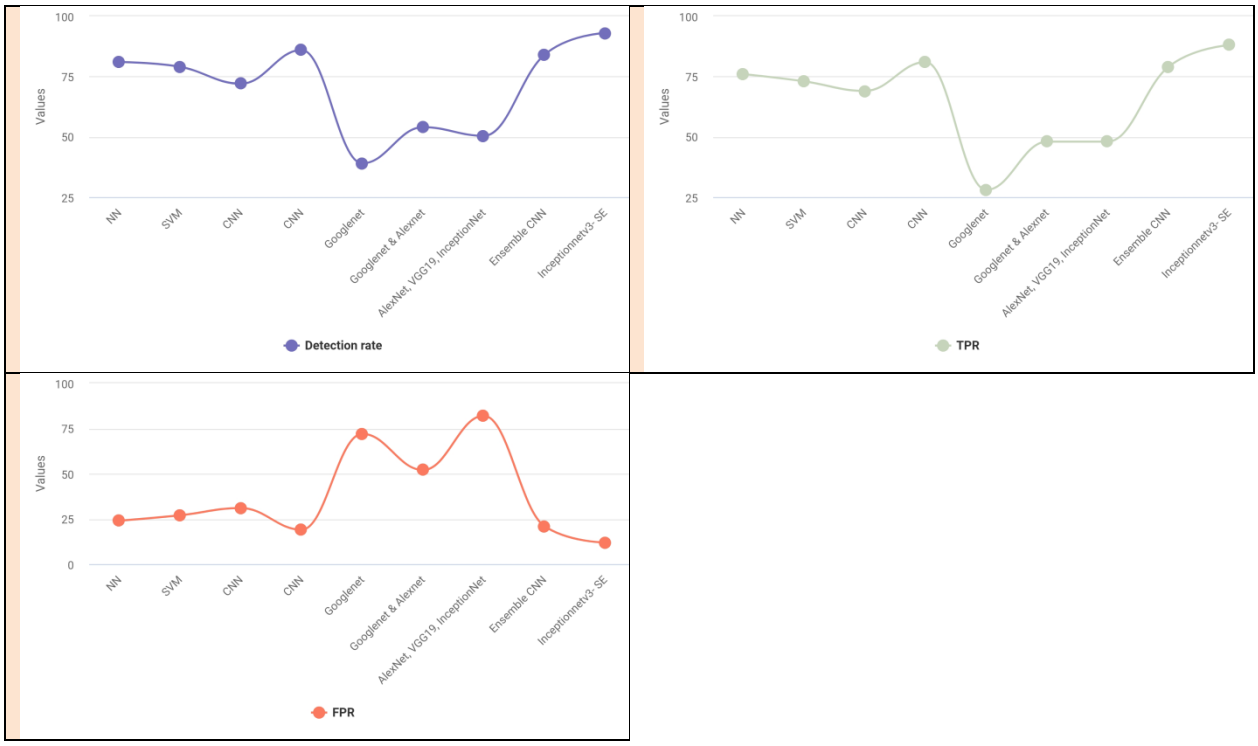

Figure 11: Models vs Measures over a) detection rate, b) TPR, c) FPR

The findings reveal that the suggested approach is extremely efficient. It has been demonstrated that implementing the recommended strategy for early tumor identification improves clinical practice quality and accuracy. The suggested approach for tumor monitoring has been developed to assist pathologists in determining the specific tumor area and kind of tumor.

5. Conclusion

Timely identification of pneumonia is vital for selecting appropriate treatment and preventing the disease from posing a risk to the patient's life. Although chest radiographs are the most used tool for diagnosing pneumonia, they are subject to inter-class variability and rely on the clinician's expertise in identifying early signs of pneumonia. To aid medical professionals, this study has developed an automated CAD system that utilizes deep transfer learning-based classification to categorize chest X-ray images into two categories: "Pneumonia" and "Normal." An SE-CNN model for early-stage identification of pneumonia was provided in this research. To increase the network's performance, numerous adjustments were made to the pre-trained Inception V3Net network and preprocessing was used. As a result, our network was able to detect pneumonia at an early stage, better than current state-of-the-art networks, when trained on the Kermany dataset and RSNA Pneumonia Detection Challenge dataset. When compared to the existing classification approach, the suggested classification method had the highest accuracy of 91.56%. Further, we found that our network had 91.56 % accuracy, 91 % f1-score, 91 per cent recall, and 91.96 per cent quadratic weighted KAPPA, respectively. These experimental findings indicate that our approach can be used in clinical settings for pneumonia detection.

References

[1] Rajpurkar, Pranav, Jeremy Irvin, Kaylie Zhu, Brandon Yang, Hershel Mehta, Tony Duan, Daisy Ding et al. "Chexnet: Radiologist-level pneumonia detection on chest x-rays with deep learning." *arXiv preprint arXiv:1711.05225* (2017).

[2] Gabruseva, Tatiana, Dmytro Poplavskiy, and Alexandr Kalinin. "Deep learning for automatic pneumonia detection." In *Proceedings of the IEEE/CVF Conference on Computer Vision and Pattern Recognition Workshops*, pp. 350-351. 2020.

Doi: https://doi.org/10.54216/FPA.160110

Received: July 15, 2023 Revised: November 15, 2023 Accepted: April 28, 2024

[3] Chouhan, Vikash, Sanjay Kumar Singh, Aditya Khamparia, Deepak Gupta, Prayag Tiwari, Catarina Moreira, Robertas Damaševičius, and Victor Hugo C. De Albuquerque. "A novel transfer learning based approach for pneumonia detection in chest X-ray images." *Applied Sciences* 10, no. 2 (2020): 559.
[4] Fiszman, Marcelo, Wendy W. Chapman, Dominik Aronsky, R. Scott Evans, and Peter J. Haug. "Automatic detection of acute bacterial pneumonia from chest X-ray reports." *Journal of the American Medical Informatics Association* 7, no. 6 (2000): 593-604.
[5] Pan, Ian, Alexandre Cadrin-Chênevert, and Phillip M. Cheng. "Tackling the radiological society of North America pneumonia detection challenge." *American Journal of Roentgenology* 213, no. 3 (2019): 568-574.
[6] Paras Lakhani and Baskaran Sundaram. 2017. Deep learning at chest radiography: automated classification of pulmonary tuberculosis by using convolutional neural networks. Radiology 284, 2 (2017), 574582
[7] Kai-Lung Hua, Che-Hao Hsu, Shintami Chusnul Hidayati, WenHuang Cheng, and Yu-Jen Chen. 2015. Computer-aided classification of lung nodules on computed tomography images via deep learning technique. OncoTargets and Therapy 8 (2015).
[8] Aswathy S U, Abraham A. A Review on State-of-the-Art Techniques for Image Segmentation and Classification for Brain MR Images. Current Medical Imaging. 2022 Apr. DOI: 10.2174/1573405618666220426100944.
[9] Aswathy S U, Abraham A. A Review on State-of-the-Art Techniques for Image Segmentation and Classification for Brain MR Images. Current Medical Imaging. 2022 Apr. DOI: 10.2174/1573405618666220426100944. PMID: 35473525.
[10] S. U., A.; P. P., F.R.; Abraham, A.; Stephen, D. Deep Learning-Based BoVW–CRNN Model for Lung Tumor Detection in Nano-Segmented CT Images. *Electronics* **2023**, *12*, 14. https://doi.org/10.3390/electronics12010014
[11] Xiaosong Wang, Yifan Peng, Le Lu, Zhiyong Lu, Mohammadhadi Bagheri, and Ronald M Summers. 2017. Chestx-ray8: Hospital-scale chest x-ray database and benchmarks on weakly-supervised classification and localization of common thorax diseases. In Computer Vision and Pattern Recognition (CVPR), 2017 IEEE Conference on. IEEE, 34623471
[12] Varshni, D., Thakral, K., Agarwal, L., Nijhawan, R., & Mittal, A. (2019, February). Pneumonia detection using CNN based feature extraction. In *2019 IEEE International Conference on Electrical, Computer and Communication Technologies (ICECCT)* (pp. 1-7). IEEE.
[13] Rahman, Tawsifur, Muhammad EH Chowdhury, Amith Khandakar, Khandaker R. Islam, Khandaker F. Islam, Zaid B. Mahbub, Muhammad A. Kadir, and Saad Kashem. "Transfer learning with deep convolutional neural network (CNN) for pneumonia detection using chest X-ray." *Applied Sciences* 10, no. 9 (2020): 3233.
[14] GM, HARSHVARDHAN, MAHENDRA KUMAR Gourisaria, SIDDHARTH SWARUP Rautaray, and M. A. N. J. U. S. H. A. Pandey. "Pneumonia detection using CNN through chest X-ray." *Journal of Engineering Science and Technology (JESTEC)* 16, no. 1 (2021): 861-876.
[15] Kermany, D.S.; Goldbaum, M.; Cai, W.; Valentim, C.C.S.; Liang, H.; Baxter, S.L.; McKeown, A.; Yang, G.; Wu, X.; Yan, F.; Dong, J.; Prasadha, M.K.; Pei, J.; Ting, M.Y.L.; Zhu, J.; Li, C.; Hewett, S.; Dong, J.; Shi, W.; Fu, X.; Duan, Y.; Huu, V.A.N.; Wen, C.; Zhang, E.D.; Zhang, C.L.; Li, O.; Wang, X.; Singer, M.A.; Sun, X.; Xu, J.; Tafreshi, A.; Lewis, M.A.; Xia, H.; and Zhang, K. (2018). Identifying medical diagnoses and treatable diseases by image-based deep learning. Cell, 172(5), 1122-1131.
[16] Rajpurkar, P.; Irvin, J.; Zhu, K.; Yang, B.; Mehta, H.; Duan, T.; Ding, D.; Bagul, A.; Langlotz, C.; Shpanskaya, K.; Lungren, M.P.; and Ng, A.Y. (2017). Chexnet: Radiologist-level pneumonia detection on chest x-rays with deep learning. arXiv preprint arXiv:1711.05225.
[17] Pankratz, D.G.; Choi, Y.; Imtiaz, U.; Fedorowicz, G.M.; Anderson, J.D.; Colby, T.V.; Myers, J.L.; Lynch, D.A.; Brown, K.K.; Flaherty, K.R.; Steele, M.P.; Groshong, S.D.; Raghu, G.; Barth, N.M.; Walsh, P.S.; Huang, J.; Kennedy, G.C.; and Matinez, F.J. (2017). Usual interstitial pneumonia can be detected in transbronchial biopsies using machine learning. Annals of the American Thoracic Society (ATS), 14(11), 1646-1654.
[18] Caruana, R.; Lou, Y.; Gehrke, J.; Koch, P.; Sturm, M.; and Elhadad, N. (2015). Intelligible models for healthCare. Proceedings of the 21st ACM SIGKDD International Conference on Knowledge Discovery and Data Mining (KDD '15). 1721-1730.
[19] Wang, X.; Peng, Y.; Lu, L.; Lu, Z.; Bagheri, M.; and Summers, R.M. (2017). Chestx-ray8: Hospital-scale chest x-ray database and benchmarks on weakly-supervised classification and localization of common thorax

Doi: https://doi.org/10.54216/FPA.160110

Received: July 15, 2023 Revised: November 15, 2023 Accepted: April 28, 2024

diseases. Proceedings of the IEEE Conference on Computer Vision and Pattern Recognition. Honolulu, HI, 3462-3471

[20] Stephen, Okeke, Mangal Sain, Uchenna Joseph Maduh, and Do-Un Jeong. "An efficient deep learning approach to pneumonia classification in healthcare." *Journal of healthcare engineering* 2019 (2019).

[21] Roy, Abhijit Guha, Nassir Navab, and Christian Wachinger. "Recalibrating fully convolutional networks with spatial and channel "squeeze and excitation" blocks." *IEEE transactions on medical imaging* 38, no. 2 (2018): 540-549.

[22] undo, Leonardo, Changhee Han, Yudai Nagano, Jin Zhang, Ryuichiro Hataya, Carmelo Militello, Andrea Tangherloni et al. "USE-Net: Incorporating Squeeze-and-Excitation blocks into U-Net for prostate zonal segmentation of multi-institutional MRI datasets." *Neurocomputing* 365 (2019): 31-43.

[23] Li, Xia, Jianlong Wu, Zhouchen Lin, Hong Liu, and Hongbin Zha. "Recurrent squeeze-and-excitation context aggregation net for single image deraining." In *Proceedings of the European conference on computer vision (ECCV)*, pp. 254-269. 2018.

[24] Hu, Yang, Guihua Wen, Mingnan Luo, Dan Dai, Jiajiong Ma, and Zhiwen Yu. "Competitive inner-imaging squeeze and excitation for the residual network." *arXiv preprint arXiv:1807.08920* (2018).

[25] Zhong, Xian, Oubo Gong, Wenxin Huang, Lin Li, and Hongxia Xia. "Squeeze-and-excitation wide residual networks in image classification." In *2019 IEEE International Conference on Image Processing (ICIP)*, pp. 395-399. IEEE, 2019.

[26] Cheng, Xi, Xiang Li, Jian Yang, and Ying Tai. "SESR: Single image super-resolution with a recursive squeeze and excitation networks." In *2018 24th International conference on pattern recognition (ICPR)*, pp. 147-152. IEEE, 2018.

[27] Verma, Devvret, Chitransh Bose, Neema Tufchi, Kumud Pant, Vikas Tripathi, and Ashish Thapliyal. "An efficient framework for identification of Tuberculosis and Pneumonia in chest X-ray images using Neural Network." *Procedia Computer Science* 171 (2020): 217-224.

[28] Toğaçar, M., B. Ergen, Z. Cömert, and F. Özyurt. "A deep feature learning model for pneumonia detection applying a combination of mRMR feature selection and machine learning models." *IRBM* 41, no. 4 (2020): 212-222.

[29] Sukumaran, A. and Abraham, A., 2022. Automated Detection and Classification of Meningioma Tumor from MR Images Using Sea Lion Optimization and Deep Learning Models. *Axioms*, *11*(1), p.15.

[30] Ko, Heewon, Hyunsoo Ha, Hyuna Cho, Kiwon Seo, and Jihye Lee. "Pneumonia detection with a weighted voting ensemble of CNN models." In *2019 2nd International Conference on Artificial Intelligence and Big Data (ICAIBD)*, pp. 306-310. IEEE, 2019.

[31] Sirish Kaushik, V., Anand Nayyar, Gaurav Kataria, and Rachna Jain. "Pneumonia detection using Convolutional Neural Networks (CNNs)." In *Proceedings of First International Conference on Computing, Communications, and Cyber-Security (IC4S 2019)*, pp. 471-483. Springer, Singapore, 2020.

[32] Ullah, Muhammad Saad, Huma Qayoom, and Farman Hassan. "Viral Pneumonia Detection Using Modified GoogleNet Through Lung X-rays." In *2021 4th International Symposium on Advanced Electrical and Communication Technologies (ISAECT)*, pp. 1-6. IEEE, 2021.

[33] Özsoy, Yaren, and Deniz Taşkin. "Comparison of Deep Learning Models AlexNet and GoogLeNet in Detection of Pneumonia and Covid19." In *2021 International Conference on Engineering and Emerging Technologies (ICEET)*, pp. 1-3. IEEE, 2021.

[34] Bhandary, Abhir, G. Ananth Prabhu, V. Rajinikanth, K. Palani Thanaraj, Suresh Chandra Satapathy, David E. Robbins, Charles Shasky, Yu-Dong Zhang, João Manuel RS Tavares, and N. Sri Madhava Raja. "Deep-learning framework to detect lung abnormality–A study with chest X-Ray and lung CT scan images." *Pattern Recognition Letters* 129 (2020): 271-278.

[35] Das, Dipayan, K. C. Santosh, and Umapada Pal. "Truncated inception net: COVID-19 outbreak screening using chest X-rays." *Physical and engineering sciences in medicine* 43, no. 3 (2020): 915-925.

Doi: https://doi.org/10.54216/FPA.160110

Received: July 15, 2023 Revised: November 15, 2023 Accepted: April 28, 2024